Pre-print

Sun, W., Zhao, L., Malusà, M. G., Guillot, S., & Fu, L. Y. (2019). 3-D Pn tomography reveals continental subduction at the boundaries of the Adriatic microplate in the absence of a precursor oceanic slab. Earth and Planetary Science Letters, 510, 131-141.

https://doi.org/10.1016/j.epsl.2019.01.012

3-D Pn tomography reveals continental subduction at the boundaries of the Adriatic microplate in the absence of a precursor oceanic slab

Weijia Sun[1,6*], Liang Zhao[2], Marco G. Malusà[3*], Stéphane Guillot[4], Li-Yun Fu[5]

1. Key Laboratory of Earth and Planetary Physics, Institute of Geology and Geophysics, Chinese Academy of Sciences, Beijing 100029, China.
2. State Key Laboratory of Lithospheric Evolution, Institute of Geology and Geophysics, Chinese Academy of Sciences, Beijing 100029, China.
3. Department of Earth and Environment Sciences, University of Milano-Bicocca, Milan, Italy.
4. Univ. Grenoble Alpes, Univ. Savoie Mont Blanc, CNRS, IRD, IFSTTAR, ISTerre, 38000 Grenoble, France.
5. School of Geosciences, China University of Petroleum (East China), Qingdao, Shandong 266580, China.
6. Institutions of Earth Science, Chinese Academy of Sciences, Beijing 100029, China.

* Authors for correspondence: Weijia Sun (swj@mail.iggcas.ac.cn); Marco G. Malusà (marco.malusa@unimib.it)

Abstract Slab pull generated by subducting oceanic lithosphere is generally considered as a major trigger for the onset of continental subduction. However, this may be in conflict with the occurrence of UHP terranes bearing no evidence of oceanic lithospheric rocks involved in the exhumation cycle. Here, we image the uppermost mantle P velocity structure beneath the Central Mediterranean, suggesting the possibility that the initiation of continental subduction may not require a precursor oceanic slab. We combine (i) a three-step inverted 3-D Pn tomography model of the Adriatic microplate with (ii) available geologic constraints and palinspastic reconstructions of the Africa-Eurasia plate-boundary zone. Our Pn tomography model reveals elongated regions with Vp <7.6 km/s around the Adriatic microplate, clearly connected with the slab structure inferred from teleseismic P wave tomography and supportive of continental subduction along the Dinaric, Alpine and Apenninic subduction zones. Contrasting styles of subduction are observed on the opposite sides of the Adriatic microplate: a laterally variable SW-dipping subduction is documented beneath the Apennines, continental to the north and oceanic to the south, where rollback is faster; a laterally continuous NE-dipping continental subduction is documented under the Dinarides. The lack of a precursor oceanic slab under the Dinarides demonstrates that the onset of continental subduction, in complex plate-boundary zones, can be controlled by plate-tectonic processes far away from the subduction initiation site, and may take place without the contribution of the negative buoyancy of an old oceanic lithosphere.

1. Introduction

Continental subduction has long been dismissed in the light of the intrinsic buoyancy of continental crust (McKenzie 1969) but it is now considered as a relatively common geodynamic process, either demonstrated by the occurrence of ultra-high pressure (UHP) metamorphic rocks of continental origin exposed at the Earth's surface (e.g., Guillot et al., 2009 and references therein) or by high-resolution geophysical imagery (e.g., Schneider et al., 2013; Zhao et al., 2015). The driving force for continental subduction is generally thought to be provided by the negative buoyancy of old oceanic lithosphere that enters the subduction zone before the adjoining continental margin (e.g., Davies, 1999). However, there are examples of UHP terranes that bear no evidence of oceanic lithosphere involved in the exhumation cycle, e.g., the Dabie Shan in China (Zhang et al., 2009) or the Western Gneiss Region in Norway (Hacker, 2007). This may either suggest that the negative buoyancy of eclogitized oceanic lithosphere is too high to permit its partial exhumation, or that the continental subduction does not necessarily need the trigger of a large oceanic slab. And in some specific cases the role of slab pull may be negligible to enhance the subduction (e.g., Guillaume et al., 2013). Such a challenging scenario requires validation in a well-constrained subduction setting where the physiography of the subducting plate is independently assessed, and the occurrence of a precursor oceanic slab can be safely excluded.

The Adriatic microplate, located within the complex plate boundary zone between Africa and Eurasia (e.g., Faccenna et al., 2014) is an ideal setting to test this hypothesis (Fig. 1a). This microplate is bounded by three orogenic belts (Alps, Apennines and Dinarides) mainly formed during Cenozoic subductions (e.g., Handy et al., 2010; Malusà et al., 2015), and the physiography inherited from the Mesozoic opening of the Alpine Tethys is exceptionally well preserved (e.g., Winterer and Bosellini, 1981; Fantoni and Franciosi, 2010). However, along the boundaries of the Adriatic microplate, UHP rocks attesting Cenozoic continental subduction are only observed atop the European slab in the Western Alps (Handy et al., 2010; Zhao et al., 2015). No Adria-derived UHP rock has been exhumed in the Apenninic and Dinaric belts (Jolivet et al., 2003; Ustaszewski et al., 2008; Malusà et al., 2015), which means that the occurrence of Adriatic continental crust possibly reaching mantle depths has to be confirmed by geophysical evidence.

In this article, we employ the inversion of Pn phases to map the seismic velocity signature of continental subduction along the boundaries of the Adriatic microplate. Pn phases, the first arrivals at regional distance, propagate through the crust, penetrate into the uppermost mantle and are finally refracted through the Moho (e.g., Hearn, 1999) and return to the free surface. Geophysical images based on the analysis of Pn phases are already available for the Mediterranean region (e.g., Pei et al., 2011; Diaz et al., 2013; Lü et al., 2017), but these images have low resolution and are based on a 2-D inversion scheme (Hearn, 1999) that strongly depends on crustal depth corrections. This implies that large errors may affect the inversion of these Pn datasets, especially in complicated tectonic settings as the Africa-Eurasia plate boundary zone. Here we apply a three-step Pn traveltime inversion scheme to invert the 3-D wavespeed structure of the uppermost mantle beneath the Adriatic microplate using Pn arrivals recorded since the 1960s by permanent and temporary stations (Fig. 1b). The resulting 3-D tomography model with resolution of $0.75^{o} \times 0.75^{o}$, when interpreted within the framework of available geologic and geodynamic constraints, provides seismic evidence of continental subduction in the lack of a precursor oceanic slab, with implications for our understanding of subduction processes in general.

2. Tectonic setting

The Adriatic microplate is the result of breakup of the northern Gondwana margin and consequent opening of the Alpine Tethys in the Jurassic (e.g., Handy et al., 2018; von Raumer et al., 2013). The architecture inherited from the Mesozoic Tethyan rifting is largely preserved within the major thrust sheets of the Southern Alps, the Apennines and the Dinarides (Fig. 1a), and it is also imaged by oil-industry surveys beneath the Cenozoic sedimentary successions of the Po Plain and the Adriatic Sea (e.g., Fantoni and Franciosi, 2010). Beneath the Po Plain, the Adriatic microplate preserves evidence of a series of Mesozoic platforms, ridges and plateaus (e.g., Lugano ridge and Trento plateau) separated by NNE-SSW trending basins floored by continental crust (e.g., Lombardian and Belluno basins) (Figs. 1a, 2a). At the boundary with the Western Alps, a NNE-SSW trending gravimetric anomaly, classically referred to as the Ivrea body (IV in Fig. 1a; Nicolas et al., 1990), likely marks the lithospheric necking zone of the southern Tethyan margin (Malusà et al., 2015). Long-lasting carbonate platforms (Apulian, Dalmatia and Latium-Abruzzi) are preserved to the SE, where they are separated by an elongated basin floored by continental crust (Adriatic basin in Fig. 1a). Mesozoic oceanic crust is preserved farther south in the Ionian basin (Fig. 1a).

The NNE-SSW structural grain inherited from Tethyan rifting shares the same orientation with several major faults mapped in the Alpine and Apenninic wedges (Fig. 1a). For example: the westernmost segment of the Insubric Fault (IF in Fig. 1a) is aligned to the Ivrea body in the Western Alps; the Giudicarie Fault (GF in Fig. 1a) is located at the boundary between the Mesozoic Lombardian basin and the Trento plateau; the NNE-SSW faults at the transition between the Northern and the Southern Apennines bound the Mesozoic Latium-Abruzzi platform (Fig. 1a).

The WNW-ESE trend of the Insubric Fault in the Eastern Alps may mirror the orientation of transform faults at the time of continental breakup, and a similar trend has been also proposed for the original boundary between the Adriatic continental crust and the Ionian oceanic crust farther south (Faccenna et al. 2014) (Fig. 2b, c). Within this scenario, the inferred Mesozoic spreading direction for the Adriatic margin would be nearly perpendicular to the direction of Adria-Europe convergence documented since the Late Cretaceous by paleomagnetic data (purple arrows in Fig. 2b, c). In the Late Cretaceous, oceanic domains were thus expected to be present to the NW of the Adriatic microplate, in front of the incipient Alpine and Apenninic subduction zones, but not in correspondence with the future Dinarides.

Adria-Europe convergence in the Late Cretaceous was initially accommodated by SE-dipping Alpine subduction (e.g., Handy et al., 2010) and by progressive consumption of the Alpine Tethys and adjoined European paleomargin beneath the Adriatic microplate. The Apenninic and Dinaric subduction zones started developing along the western and eastern boundaries of the Adriatic microplate during the Paleogene (Fig. 2b). The Apenninic slab progressively shifted northward beneath Corsica-Sardinia (Malusà et al., 2015), and started interacting with the European slab by the end of the Oligocene (Malusà et al., 2016; Zhao et al., 2016), when the onset of Apenninic slab retreat determined the Neogene opening of the Ligurian-Provençal and Tyrrhenian backarc basins (Faccenna et al., 2014) (Fig. 2c). Apenninic slab retreat is associated with a progressive migration of calc-alkaline magmatism in the Apenninic forearc (Peccerillo and Frezzotti, 2015). A number of buried thrust fronts (a-to-d in Fig. 1a) developed during ongoing Adria-Europe convergence in front of the Northern Apennines (Malusà and Balestrieri, 2012), where the Plio-Quaternary sedimentary successions of the Po Plain record differential subsidence along the orogen strike (Bigi et al., 1990). Cenozoic continental subduction, well documented by geophysical data in the Western Alps and in the Apennines (Chiarabba et al., 2014; Zhao et al., 2015), still remains conjectural and poorly constrained in the Eastern Alps and the Dinarides.

3. Methods and datasets

The Pn tomography model presented in this work is based on the three-step 3-D approach proposed by Sun and Kennett (2016a; 2016b). The main steps of this approach include: (i) building of a 3-D broad-scale initial model; (ii) relocating all the events by a nonlinear relocator in the 3-D initial model; and (iii) performing traveltime residuals inversion in spherical coordinates.

3.1 The 3-D initial model

A good 3-D initial model can significantly speed up the convergence of tomographic inversion, thus reducing the computational burden and the variance of traveltime residuals (see supplementary material). Our 3-D model is defined on a regular computational grid interval of 0.25° in longitude (from 1°W to 22°E) and latitude (from 38°N to 52°N) and 5 km in depth (from 0 to 280 km) in the spherical coordinate system, for a total of ~0.3 million grids. The Pn phases propagate from the source in the crust to the uppermost mantle and are refracted back to the crust due to vertical velocity gradients.

A good crustal velocity model may thus enhance the reliability of inversion of uppermost mantle velocities. The EPcrust model (Molinari and Morelli, 2011), which integrates a range of previous data by previous authors, provides a reliable image of continental-scale crustal properties, but locally underestimates the Moho depth. For example beneath the Western Alps (<40 km instead of ~40-70 km as inferred from recent receiver function analysis by Zhao et al., 2015). The ESC Moho model of Grad et al. (2009) better agrees with the recent results of Zhao et al. (2015), and is also considered to define the crust components of the 3-D initial model (Fig. 3).

For the mantle components, we use a mantle P velocity model derived from the global shear wavespeed model SL2013sv (Schaeffer and Lebedev, 2013) using the empirical relations. The P velocity deviations are first converted from the S velocity deviations relative to the ak135 model (Kennett et al., 1995) and then the absolute P velocities are obtained from summation between the P deviations and the ak135 model. This procedure was successfully tested in recent studies dealing with the inversion of uppermost mantle structures beneath Australia (Sun and Kennett, 2016a) and eastern China (Sun and Kennett, 2016b).

3.2 Pn arrival data

Pn phases sample deeper levels of the uppermost mantle as the epicentral distance of events becomes larger. In our study, the region under consideration is sufficiently wide to allow the penetration of Pn with long epicentral distance into the uppermost mantle. Figure 4 compares the Pn raypaths in the 1-D ak135 model and in the 3-D initial and inverted velocity models. In the 1-D model, the Pn phases propagate downward to 50 km at most at an epicentral distance of 10°, whereas in both 3-D models the Pn phases dive to ~100 km depth. This illustrates that the actual Pn wave propagation is much more complicated than the simplified assumption of running along paths immediately below the Moho, as expected for a stratified medium.

In this study, we used the Pn arrivals for events with magnitude > 3.0 archived at the International Seismological Centre (ISC, http://www.isc.ac.uk) from January 1960 to November 2013. The waveforms of events with magnitude > 3.5 recorded from December 2013 to November 2016 were fetched from the EIDA Data Archives at GEOFON (http://www.webdc.eu/webdc3/). We also collected events recorded during the CIFALPS experiment in the Western Alps from July 2012 to September 2013, in order to improve the ray path coverage in the complex Alps-Apennines transition zone (Malusà and Balestrieri, 2012; Malusà et al., 2017). The first arrivals were first automatically picked using the autoregressive technique applied to Z-component traces (Leonard and Kennett, 1999). Then, all the automatically picked arrivals were examined visually and calibrated manually, and only arrivals with clear onsets were selected.

We performed rigid selections of available Pn arrivals before inverting the uppermost mantle structures. The first arrivals with epicentral distance between 2.0°

and 12° were considered to be Pn arrivals, which screen out the possible Pg phases at shorter epicentral distances. We also excluded any raypaths with Pn traveltime residuals larger than 8 s relative to the ak135 model (Kennett et al., 1995) to avoid erroneous pickings and other inconsistencies, although the 3-D model can tolerate larger residuals with considerations of lateral velocity perturbations. We dropped events with location differences greater than 10 km when comparing catalogue and relocation in the 3-D initial model (see following section), and kept the earthquake clusters of Fig. 1b to enhance the reliability of inverted Pn wavespeed. This led to a final dataset of 395,918 selected Pn arrivals for 9,519 events and 1,080 stations.

3.3 Event relocation

Focal parameters influence the traveltime of regional phases. These parameters are determined using different models, such as the JB Earth model for events archived at ISC before 2006, and the ak135 model for events archived since January 1st 2006. In order to eliminate potential bias in Pn traveltime using different models, we have relocated all the events from 1960 to 2016 by a nonlinear event locator using the 3-D initial model.

The nonlinear event locator precomputed the seismic traveltime at all 3-D grids for all permanent and portable stations using the multi-stage fast marching method (FMM) (de Kool et al., 2006). All parameters are defined on the regular grids in the spherical coordinates leading to avoid the Earth flatten approximation at regional scale. The predicted traveltime at an arbitrary location in the 3-D model is obtained by trilinear interpolation, and the four focal parameters (i.e., origin time, two epicenteral parameters and depth) are determined by the fully nonlinear Neighborhood Algorithm (NA, Sambridge and Kennett, 2001). According to previous studies (de Kool and Kennett, 2014; Sun and Kennett, 2016a), this procedure of relocating events in a 3-D model before regular Pn tomography can effectively decrease the variance of traveltime residuals. In the study area, earthquake relocation reduced the variance of traveltime residuals from 10.8 to 1.99 (see supplementary material).

3.4 Inversion of Pn arrivals

We used the Fast Marching TOMOgraphy (FMTOMO) scheme (Rawlinson and Urvoy, 2006), a nonlinear tomography approach assuming local linearity, to invert the uppermost mantle P velocity structures from Pn traveltime residuals. The FMTOMO package can simultaneously invert multiple classes of body wave datasets including refractions, reflections and teleseismic data from passive and active source datasets. The multi-stage FMM (de Kool et al., 2006) is designed to solve the forward problem of traveltime prediction in the 3-D model. The algorithm is the same used for event relocation, which makes traveltime predictions compatible in the two procedures.

The subsurface inversion scheme is applied to minimize the objective function. The parametrisation is defined in 3-D spherical coordinates to avoid the Earth flatten approximation, which makes the FMTOMO approach suitable to solve regional and global tomography problems. With the FMTOMO scheme, we inverted the 3-D P velocity model of the uppermost mantle with resolution as high as 0.75°×0.75°. During the Pn tomography, we allowed the crustal velocity to be updated so that the effects of velocity variations of the crust on the uppermost mantle were taken into account. A series of inversions with different damping and smoothing regularizations were performed to determine the optimal regularization, which was reached with damping and smoothing factors equal to 20. We performed 17 iterations of inverting Pn traveltime residuals. As shown in Fig. S2, the inversion converged after the first four iterations.

4. Resolution tests

We used the checkerboard approach to examine the ability of available data and FMTOMO scheme to discern small velocity heterogeneities in the uppermost mantle. By considering the variations of Moho topography and the 3-D crustal and mantle velocities, we placed a layered checkerboard velocity anomaly overlaid on the 3-D initial model beneath the Moho (see Figs. 5b, c). This setting is much different from the traditional one with alternating fixed layers of velocity anomaly, which is not a realistic representation of the heterogeneous Earth (e.g., Fichtner et al., 2009).

We followed a well-established procedure: 1) taking the checkerboard perturbed velocity as true model and synthesizing the traveltime using the same source-station configuration of the real data; 2) applying the inversion from the 3-D initial model and synthetic residuals. In the resolution tests, the velocity anomaly ranges from -0.3 km/s to 0.3 km/s, about 3.75% perturbation from the globally average velocity in the uppermost mantle. We reduced the smoothing and damping parameters to 5 to balance the tradeoff between the resolution of data and the proximity of the inverted model to the starting model. Figure 5a illustrates the recovered checkerboard with one-layered velocity anomaly centered at depth of 50 km, and the corresponding vertical sections along latitude and longitude are displayed in Figs. 5b, c. The checkerboard patterns are recovered quite well beneath the Adriatic microplate at resolution of 0.75°×0.75°.

The resolution is poorer for the northern and eastern margins of the study region, and for the area to the SW of the Italian peninsula. For this reason, only the region between 4°E-20°E and 38°N-48°N with raypath density greater than 1000 is considered for further interpretation. These resolution tests suggest that the 3-D FMTOMO inversion scheme can readily identify not only lateral changes, but also vertical changes in P wavespeed within the Adriatic microplate, based on the fact the regional phases dive deeper at larger distances (see Fig. 4). However, the size of the well-resolved area gets progressively smaller with increasing depth (Figs. 6a, b), because of less seismic rays sampling the deeper uppermost mantle (Fig. 4c).

5. Results and interpretation

5.1 Seismic signature of continental subduction around the Adriatic microplate

The 3-D Pn wavespeed structure of the Adriatic microplate is illustrated in Fig. 7, by three horizontal slices of the inverted 3-D P velocity model, corresponding to depths of 50, 60 and 70 km. Four representative cross-sections of the initial and inverted models are shown in Fig. 8.

In our 3-D Pn tomography model, the expected seismic velocity signature of continental subduction in the upper mantle is given by P velocities <7.8 ± 0.2 km/s. Vp values >8 km/s should in fact characterize the dry peridotites of the Alpine lithospheric mantle (e.g., Solarino et al., 2018), whereas the heterogeneous Adriatic lower crust may yield Vp values ranging between ~6.7 km/s (for granulites with felsic to intermediate composition) to ~7.2 km/s (for granulite-facies metapelites), increasing up to ~7.6 km/s because of metamorphic phase changes and progressive eclogitization during subduction at depth >40 km (e.g., Solarino et al., 2018 and references therein). Oceanic subduction likely remains undetected in our tomography model, because of the high Vp values characterizing the oceanic crust after eclogitization (Vp >8.0 km/s for mafic eclogites), which are virtually undistinguishable from the Vp values characterizing the lithospheric mantle of the upper plate.

Elongated regions characterized by Vp <7.8 km/s (and locally <7.6 km/s) are observed, in Fig. 7, all along the southwestern, northwestern and northeastern borders of the Adriatic microplate. In the Alps, a low Vp belt is confined between the south- to east-dipping frontal Alpine thrusts and the north-dipping thrusts of the Adriatic retroforeland (Fig. 7a). To the south, two belts of low Vp match the frontal thrusts of the Northern Apennines and the Dinarides. We interpret these low Vp belts as the evidence of continental subduction at the boundaries of the Adriatic microplate along the Dinaric, Alpine and Apenninic subduction zones.

5.2 Continental subduction in cross section

Our Pn traveltime inversion, when analyzed in cross section and compared to the initial broad-scale velocity model (reported in the left panel of Fig. 8), introduces additional velocity heterogeneities that are shown in the right panel of Fig. 8. In cross-section A-A’, Vp <7.6 km/s can be traced down to depths >70 km beneath the

Northern Apennines, and down to depths >65 km beneath the Dinarides (yellow-to red colors in Fig. 8). The wedge-shaped yellow-to-red regions in cross-section A-A' are asymmetric. They document Adriatic continental crust located more than 20 km deeper than the Moho (i.e., the 7.8 km/s velocity interface) imaged at the western and eastern boundaries of cross-section A-A'. These findings are not consistent with simple crustal shortening across the Dinarides and the Northern Apennines, but are instead supportive of opposite-dipping continental subduction zones at the northeastern and southwestern boundaries of the Adriatic microplate (DS and AS in Fig. 8).

Cross-section B-B' highlights a progressive northward deepening of the 7.8 km/s velocity interface along the orogen strike of the Apennines, from ~40 km in the Southern Apennines to >70 km in the Northern Apennines.

The heterogeneities in P velocity observed along cross-section C-C' are consistent with an eastward-dipping continental subduction beneath the Western Alps (WA in Fig. 8), in agreement with receiver function results (Zhao et al., 2015). On the upper plate side of the Western Alps subduction, the 7.8 km/s velocity interface gets shallower in correspondence with the Ivrea body (IV in Fig. 8), in agreement with recent local earthquake tomography results (Solarino et al., 2018), and reaches a depth of ~50 km beneath the eastern Po Plain.

Cross-section D-D' highlights the relationships between the Apenninic subduction (AS in Fig. 8) and the southward-dipping Central Alps subduction (CS in Fig. 8), providing further evidence supporting the complex lithospheric structure beneath the Po Plain recently described by Malusà et al. (2018).

5.3 Along-strike changes in Pn velocity structure

The most relevant along-strike changes in velocity structure observed in the Pn tomography model are indicated by bold numbers 1 to 6 in Fig. 7a. As observed in Fig. 7, the low velocity belt corresponding to Dinaric subduction displays a remarkable continuity in the 50 km depth slice from Austria to Albania, providing geophysical evidence of a laterally continuous Dinaric subduction zone. The Dinaric low-velocity belt terminates at high-angle (1 in Fig. 7) against the low-velocity belt of the Eastern Alps, which shows an ENE-WSW trend consistent with major thrust faults formed during Alpine subduction. Notably, this ENE-WSW low-velocity belt is not observed, beneath the Eastern Alps, at depths greater than 50-60 km (Fig. 7b, c).

On the northwestern edge of the Adriatic microplate, the abrupt change in orientation of the low-Vp belts (2 in Fig. 7a) marks the boundary between the Alpine and Apenninic subduction zones. Based on our tomography model, underthrusting of continental crust by Apenninic subduction can be detected as far north as the Emilia thrust front (b in Fig. 1a). Farther west, the inferred Vp values (7.7-7.8 km/s at 50 km depth) are in line with a tectonic scenario including exhumation of hydrated mantle-wedge rocks at shallow depth (Liao et al., 2018), and with the P wave velocities documented by local earthquake tomography (Solarino et al., 2018).

The low Vp belt of the Northern Apennines shows a prominent break (3 in Fig. 7a) and is displaced northeastward in correspondence with the boundary between the Emilia and Ferrara-Romagna thrust fronts (b and c, respectively, in Fig. 1a), where the thickness of the Pliocene-Quaternary foredeep successions of the Po Plain sharply increases from ~3 km to >8 km (Pieri and Groppi, 1981). Farther south, major along-strike velocity breaks are observed at the boundary between the Northern and the Southern Apennines (4 in Fig. 7a), in correspondence with major tectonic structures mapped at the surface (Fig. 1a). The low-velocity belt parallel to the Apenninic thrust fronts is no longer observed in the Southern Apennines (5 in Fig. 7a), which suggests that subduction in southern Italy was dominantly oceanic. Offshore Albania (6 in Fig. 7a), the sharp increase in Vp (>8.0 km/s) at 60 km depth may mark the presence of oceanic crust, originally located to the south of the Adriatic basin and now squeezed within the Dinaric subduction zone.

5.4 Comparison with previous images based on a 2-D inversion scheme

Previous Pn tomography models of the area analyzed in this work (e.g., Diaz et al., 2013; Lü et al., 2017) are based on 2-D inversion schemes that are prone to average the uppermost mantle structure over depth. In the model assuming isotropic propagation that was presented by Diaz et al. (2013) (see their Fig. 8a), no major linear trend of Pn velocity anomalies is observed outside of the Alps. When an anisotropic term is included in their calculation (Diaz et al., 2013, their Fig. 8b), continuous low Pn velocity anomalies are instead imaged all along the Dinarides, the Appennines of central and southern Italy, and more discontinuously in the Alps. Unlike our 3-D Pn tomography model of Fig. 7a, no along-strike change from continental to oceanic subduction was detected by Diaz et al (2013) along the Apennines, and the relationships between Alpine and Apenninic subductions are not well resolved in their model. Similar velocity features are also observed in the model presented by Lü et al. (2017), which anyway highlights a southward increase in Pn velocities from the Northern (~7.7 km/s) to the Southern (~7.8 km/s) Apennines (Lü et al., 2017, their Fig. 10). The comparison of our results with previous Pn tomography models based on 2-D inversion suggests the importance of applying a 3-D inversion scheme, which can delineate vertical velocity variations, to get the Pn wavespeed structure of the upper mantle in tectonically complicated regions.

6. Discussion

6.1 Comparison with available teleseismic P wave tomography models

In Fig. 9, the main features of our 3-D Pn tomography model are summarized and compared with the slab structure highlighted by available teleseismic P wave tomography models (Zhao et al., 2016 and references therein). Outside of the well-resolved areas of the recent Zhao et al. (2016)'s model, slab traces in Fig. 9 are based on a previous, lower-resolution tomography model by Piromallo and Morelli (2003). In this figure, we observe a good match between the slab structure inferred from teleseismic P wave tomography (thick blue lines in Fig. 9) and the sites of European and Adriatic continental subductions documented by our 3-D Pn tomography (thick brown lines in Fig. 9). Beneath the Dinarides, a NE-dipping slab was already detected by Lippitsch et al. (2003) and Zhao et al. (2016), but it was only resolved beneath the northernmost part of the Dinaric belt. Here, we provide evidence for a continuous belt of underthrust continental material down to >50 km depth from Austria to Albania, which is clearly connected with the NE-dipping slab previously imaged by teleseismic tomography beneath the Dinarides.

The relationships between the Alpine and Dinaric subductions become clearer when the pattern of continental subduction from Pn tomography is combined with the slab structure from 100 to 300 km depth as constrained by teleseismic P wave tomography (Fig. 9). At 50 km depth, the NW-SE low-velocity belt marking the NE-dipping subduction of Adriatic continental crust under the Dinarides terminates, to the north, against the ENE-WSW trending remnants of the eastern Alpine subduction zone. At 100 to 200 km depth, evidence of Alpine subduction is no longer observed beneath the Eastern Alps, but the NE-dipping Adriatic slab is instead detected farther north, beneath the remnants of the former Alpine subduction zone (see Fig. 9). This complex slab structure may possibly require a Paleogene slab-breakoff event in the Eastern Alps, an hypothesis that would deserve further geophysical investigations. To the west of the Giudicarie Fault, the trace of continental subduction inferred from Pn tomography is clearly connected with a SE-dipping European slab continuously imaged from the Central to the Western Alps, which is steeper in the vicinity of the Giudicarie Fault. In the Northern Apennines, the segmented low-Vp belt attesting SW-ward continental subduction of Adriatic crust matches with the trace of the Apenninic slab documented by teleseismic P wave tomography, where such a segmentation is not observed at 100 km or greater depths. In central Italy, at the boundary between the Northern and the Southern Apennines, the low-velocity belt marking SW-ward continental subduction is located on top of a gap in low-Vp anomaly centered at ~100 km depth, and interpreted as a possible slab window (e.g., Zhao et al., 2016).

6.2 Contrasting styles of subduction around the Adriatic microplate

Our Pn tomography model supports the idea of contrasting styles of subduction of the opposite sides of the Adriatic microplate (Fig. 10): (i) to the NE, a laterally continuous NE-dipping continental subduction is observed under the Dinarides, possibly resuming to the north an older SE-dipping Alpine subduction; and (ii) to the SE, a laterally variable subduction is documented under the Apennines, continental to the north and oceanic to the south.

This scenario is in agreement with the presence of unsubducted Mesozoic oceanic crust in the Ionian Sea offshore Calabria (Fig. 9), which contrasts with the occurrence of Adriatic continental crust under the Adriatic sea floor. An oceanic slab beneath the Southern Apennines (5 in Fig. 10) may explain the faster retreat of the southern segment of the Apenninic trench compared to the northern one (Faccenna et al., 2014), where the interaction between the Alpine and Apenninic slabs may have controlled the location of the Corsica-Sardinia pole of rotation during the scissor-type opening of the Ligurian-Provençal and Tyrrhenian backarc basins (Malusà et al., 2016). It has been long recognized that Apenninic slab rollback was responsible for the progressive migration of Cenozoic orogenic magmatism from the southern French coast to the Apennines (yellow to purple marks in Fig. 9) (e.g., Carminati and Doglioni, 2012). Notably, the laterally variable composition of rocks subducted at the Apenninic trench, as determined by our Pn tomography model, is also mirrored by contrasting geochemical compositions of Quaternary magmas that are supportive, from the Campania province to the Aeolian Islands, of a major contamination of fluids released from the Ionian slab (purple lozenges in Fig. 9) (Peccerillo and Frezzotti, 2015). The slab window located at the boundary between the Northern and the Southern Apennines (4 in Fig. 10) may have formed right at the transition between oceanic lithosphere and more buoyant continental lithosphere subducted under the Northern Apennines.

Slab retreat is obviously hindered to the north by the interaction between the Apenninic and Alpine slab (2 in Fig. 10). Differential rates of slab retreat in the Northern Apennines are possibly accommodated by lithospheric-scale tectonic discontinuities, as observed in the Pn tomography model thanks to the offset of velocity structure at the transition between the Emilia and Ferrara-Romagna thrust fronts (3 in Fig. 10). The picture provided by Pn tomography is confirmed not only by the differential subsidence in the foreland basin north of the Apennines, hosting a >8 km thick Pliocene-Quaternary succession to the east compared to only ~3 km to the west (Pieri and Groppi, 1981), but also by the along-strike variations in erosional exhumation documented in the orogenic belt by low-temperature thermochronology (Malusà and Balestrieri, 2012).

6.3 Continental subduction beneath the Dinarides without a precursor oceanic slab

Our Pn tomography model is supportive of a laterally continuous continental subduction beneath the Dinarides. Notably, the Dinaric subduction imaged by geophysical data is a relatively young feature (Paleogene) of the Adria-Europe plate boundary zone. At the time of Dinaric subduction initiation, the Tethyan oceanic crust was already largely consumed, mainly by SE-dipping Alpine subduction (Fig. 2b). Mesozoic Tethyan crust was only preserved south of Adria, and was later subducted beneath the European continental margin in front of Sardinia (Fig. 2b, c). Remnants of Tethyan oceanic crust that underwent subduction to be exhumed as (meta)ophiolites are well documented in the suture zones overlying the main slabs (dashed green lines in Fig. 9).

Based on available reconstructions of Adria physiography inherited from Mesozoic rifting (see Figs. 1, 2), we can infer that rocks subducted beneath the Dinarides, in the Paleogene Bundva-Pindos trough (e.g., Kovács et al., 2007), likely had a continental affinity. Notably, ophiolitic rocks are exposed in the Sava and Vardar units farther east, which may suggest that continental subduction was preceded by oceanic subduction (see discussion in Kovács et al., 2007). However, this latter hypothesis can be safely ruled out by considering the spatial relationships between the Dinaric slab imaged by Pn tomography, the Sava and Vardar suture zones, and the subduction-related magmatism (Fig. 9). The (meta)ophiolites mapped all along the boundaries of the Adriatic microplate systematically show a close spatial relationship with the underlying slabs, which is not observed in the case of the Dinarides. These relationships are preserved even for slabs that experienced major retreat, such as in the Apennines. Moreover, unlike the Apennines, the age of magmatism atop the Dinaric slab is not supportive of Dinaric slab retreat. We can thus conclude that the Vardar and Sava zones are relics of Mesozoic subduction zones, and that continental subduction in the Dinarides was not triggered by a precursor oceanic slab entering the subduction zone before the adjoining Adriatic paleomargin.

The joint geophysical-geologic analysis of the Adriatic microplate and surrounding areas presented in this work thus demonstrates that different styles of subduction can be expected in complex plate boundary zones such as the Mediterranean, and that the role of slab pull during the onset of continental subduction can be negligible. Although the presence of an oceanic slab may favour slab rollback, thus determining systematic relationships between trench retreat, backarc extension and magmatism as observed in the Apennines, continental subduction may also be triggered by changes in plate motion and in the force balance away from the subduction initiation site (e.g., Stern, 2004). This was likely the case of the Dinarides, where subduction was the result of convergent motion between Africa and Eurasia during coeval opening of the Atlantic Ocean, but there is no evidence of subducted oceanic lithosphere involved in the subduction-exhumation cycle. A similar mechanism may also be invoked for continental subduction in the Hindu Kush, where there has been no oceanic crust involved since at least the Late Cretaceous (e.g., Searle et al., 2001).

7. Conclusions

Our three-step 3-D Pn tomographic velocity model of the Adriatic microplate and surrounding areas, analyzed within the framework of available geologic and geodynamic constraints, leads to the following main conclusions:

- Elongated regions with Vp <7.8 km/s down to depths >50 km around the Adriatic microplate, clearly connected with the slab structure inferred from teleseismic P wave tomography, are supportive of continental subduction along the Dinaric, Alpine and northern Apenninic subduction zones.

- The NW-SE low-Vp belt marking Dinaric subduction displays a remarkable continuity at 50 km depth slice from Austria to Albania; it terminates to the north against the NNE-SSW low-Vp belt of the Eastern Alps at deeper depths, which marks the remnants of the eastern Alpine subduction zone.

- A laterally variable SE-dipping subduction is documented beneath the Apennines, continental to the north and oceanic to the south; an oceanic slab beneath the Southern Apennines may explain the faster retreat of the southern segment of the Apenninic trench.

- The lack of a precursor oceanic slab under the Dinarides demonstrates that the onset of continental subduction, in complex plate-boundary zones, do not necessarily need a major contribution of the negative buoyancy of old oceanic lithosphere, but can be triggered by plate-tectonic processes far away from the subduction initiation site.

Our results may find application to other subduction zones, where the mechanisms of continental subduction initiation are still poorly understood.

Acknowledgements

The seismic data of the CIFALPS experiment are archived at the data center of the Seismic Array Laboratory, Institute of Geology and Geophysics, Chinese Academy of Sciences, and at the data center of the French Seismologic and Geodetic Network RESIF (doi:10.15778/RESIF.YP2012). The RESIF data center also hosts the data of the PYROPE experiment (doi:10.15778/RESIF.X72010). We are most grateful to the operators of permanent broadband seismic arrays of European countries who make their data freely available through the EIDA (European Integrated Data Archive, http://www.orfeus-eu.org/eida/eida.html). Most of the permanent stations we used belong to networks CH (Switzerland Seismological Network), FR (RESIF and other broadband permanent networks in metropolitan France, doi:10.15778/RESIF.FR), GR (German Regional Seismic Network), GU (Regional Seismic Network of North Western Italy, doi:10.7914/SN/GU), IV (Italian National Seismic Network), MN (MEDNET Project), SL (Slovenia Seismic Network), and TH (Thüringer Seismisches Netz). The CIFALPS project is funded by the State Key Laboratory of Lithospheric Evolution, China. The research is sponsored by the National Key R&D Program of China (grant no 2017YFC0601206) and National Natural Science Foundation of China (grant no. 41720104006 and 41630210). Support from the Youth Innovation Promotion Association CAS (2017094) is also acknowledged. The manuscript benefited from insightful comments by the editor and two anonymous reviewers and feedback from Nicholas Rawlinson.

References

1. Bertotti, G., Picotti, V., Bernoulli, D., Castellarin, A., 1993. From rifting to drifting: Tectonic evolution of the south-Alpine upper crust from the Triassic to the Early Cretaceous, Sedimentary Geology, 86, 53–76.

2. Bigi, G., Castellarin, A., Coli, M., Dal Piaz, G. V., Sartori, R., Scandone, P., & Vai, G. B., 1990. Structural Model of Italy scale 1:500.000, sheet 1. SELCA Firenze, I: C.N.R., Progetto Finalizzato Geodinamica.

3. Carminati, E., Doglioni, C., 2012. Alps vs. Apennines: The paradigm of a tectonically asymmetric Earth. Earth-Science Reviews, 112, 67-96.

4. Chiarabba, C., Giacommuzzi, G., Bianchi, I., Piana Agostinetti, N., Park, J., 2014. From underplating to delamination-retreat in the northern Apennines. Earth and Planetary Science Letters, 403, 108-116.

5. Davies, G.F., 1999. Dynamic Earth. Cambridge University Press, New York.

6. de Kool, M., Rawlinson, N., Sambridge, M., 2006. A practical grid-based method for tracking multiple refraction and reflection phases in three-dimensional heterogeneous media. Geophysical Journal International 167, 253-270.

7. de Kool, M., Kennett, B., 2014. Practical earthquake location on a continental scale in Australia using the AuSREM 3D velocity model. Bulletin of the Seismological Society of America 104, 2755-2767.

8. Diaz, J., Gil, A., Gallart, J., 2012. Uppermost mantle seismic velocity and anisotropy in the Euro-Mediterranean region from Pn and Sn tomography. Geophysical Journal International 192, 310-325.

9. Faccenna, C., Becker, T.W., Auer, L., Billi, A., Boschi, L., Brun, J.P., Capitanio, F.A., Funiciello, F., Horvàth, F., Jolivet, L., Piromallo, C., Royden, L., Rossetti, F., Serpelloni, E., 2014. Mantle dynamics in the Mediterranean. Rev. Geophys. 52, 283–332.

10. Fantoni, R., Franciosi, R., 2010. Tectono-sedimentary setting of the Po Plain and Adriatic foreland. Rend. Lincei, 21(1), 197-209.

11. Fichtner, A., Kennett, B.L., Igel, H., Bunge, H.-P., 2009. Full seismic waveform tomography for upper-mantle structure in the Australasian region using adjoint methods. Geophysical Journal International 179, 1703-1725.

12. Guillaume, B., Husson, L., Funiciello, F., Faccenna, C., 2013. The dynamics of laterally variable subductions: laboratory models applied to the Hellenides. Solid Earth, 4, 179-200.

13. Grad, M., Tiira, T., Group, E.W., 2009. The Moho depth map of the European Plate. Geophysical Journal International 176, 279-292.

14. Guillot, S., Hattori, K., Agard, P., Schwartz, S., Vidal, O., 2009. Exhumation Processes in Oceanic and Continental Subduction Contexts: A Review, Springer, Berlin.

15. Hacker, B.R., 2007. Ascent of the ultrahigh-pressure Western Gneiss Region, Norway. Geological Society of America Special Paper 419, 171-184.

16. Handy, M.R., M. Schmid, S., Bousquet, R., Kissling, E., Bernoulli, D., 2010. Reconciling plate-tectonic reconstructions of Alpine Tethys with the geological–geophysical record of spreading and subduction in the Alps. Earth-Science Reviews 102, 121-158.

17. Hearn, T.M., 1999. Uppermost mantle velocities and anisotropy beneath Europe. Journal of Geophysical Research: Solid Earth 104, 15123-15139.

18. Jolivet, L., Faccenna, C., Goffé, B., Burov, E., Agard, P., 2003. Subduction tectonics and exhumation of high-pressure metamorphic rocks in the Mediterranean orogens. American Journal of Science 303, 353-409.

19. Kennett, B., Engdahl, E., Buland, R., 1995. Constraints on seismic velocities in the Earth from traveltimes. Geophysical Journal International 122, 108-124.

20. Kovacs, I., Csontos, L., Szabò, C, Bali, E., Falus, G., Benedek, K., Zajacz, Z., 2007. Paleogene–early Miocene igneous rocks and geodynamics of the Alpine–Carpathian–Pannonian–Dinaric region: an integrated approach. L. Beccaluva, G. Bianchini, M. Wilson (Eds.), Cenozoic volcanism in the Mediterranean area, Geological Society of America Special Paper, 418 (2007), pp. 93-112

21. Leonard, M., Kennett, B., 1999. Multi-component autoregressive techniques for the analysis of seismograms. Physics of the Earth and Planetary Interiors 113, 247-263.

22. Liao, J., Malusà, M.G., Zhao, L., Baldwin, S.L., Fitzgerald, P.G., Gerya, T., 2018. Divergent plate motion drives rapid exhumation of (ultra)high pressure rocks. Earth and Planetary Science Letters, 491, 67-80.

23. Lippitsch, R., Kissling, E., Ansorge, J., 2003. Upper mantle structure beneath the Alpine orogen from high-resolution teleseismic tomography. J Geophys Res-Sol Ea 108.

24. Lü, Y., Ni, S., Chen, L., Chen, Q.F., 2017. Pn tomography with Moho depth correction from eastern Europe to western China. Journal of Geophysical Research: Solid Earth 122, 1284-1301.

25. Malusà, M.G., Balestrieri, M.L., 2012. Burial and exhumation across the Alps-Apennines junction zone constrained by fission-track analysis on modern river sands. Terra Nova 24, 221–226.

26. Malusà, M.G., Faccenna, C., Baldwin, S.L., Fitzgerald, P.G., Rossetti, F., Balestrieri, M.L., Danišík, M., Ellero, A., Ottria, G., Piromallo, C., 2015. Contrasting styles of (U) HP rock exhumation along the Cenozoic Adria-Europe plate boundary (Western Alps, Calabria, Corsica). Geochemistry, Geophysics, Geosystems 16, 1786-1824.

27. Malusà, M.G., Anfinson, O.A., Dafov, L.N., Stockli, D.F., 2016. Tracking Adria indentation beneath the Alps by detrital zircon U-Pb geochronology: Implications for the Oligocene–Miocene dynamics of the Adriatic microplate. Geology 44, 155-158.

28. Malusà, M.G., Zhao, L., Eva, E., Solarino, S., Paul, A., Guillot, S., Schwartz, S., Dumont, T., Aubert, C., Salimbeni, S., Pondrelli, S., Wang, Q., Zhu, R., 2017. Earthquakes in the western Alpine mantle wedge. Gondwana Research 44, 89-95.

29. Malusà, M. G., Frezzotti, M. L., Ferrando, S., Brandmayr, E., Romanelli, F., Panza, G. F., 2018. Active carbon sequestration in the Alpine mantle wedge and implications for long-term climate trends. Scientific Reports, 8(1), 4740.

30. McKenzie, D.P., 1969, Speculations on the consequences and causes of plate motions: Royal Astronomical Society Geophysical Journal, v. 18, p. 1–32

31. Molinari, I., Morelli, A., 2011. EPcrust: a reference crustal model for the European Plate. Geophysical Journal International 185, 352-364.

32. Nicolas, A., Hirn, A., Nicolich, R., Polino, R., 1990. Lithospheric wedging in the western Alps inferred from the ECORS-CROP traverse. Geology 18, 587–590.

33. Peccerillo, A., Frezzotti, M., 2015. Magmatism, mantle evolution and geodynamics at the converging plate margins of Italy. Journal of the Geological Society 172, 407-427.

34. Pei, S., Sun, Y., Toksöz, M.N., 2011. Tomographic Pn and Sn velocity beneath the continental collision zone from Alps to Himalaya. Journal of Geophysical Research: Solid Earth 116.

35. Pieri, M., Groppi, G., 1981. Subsurface geological structure of the Po Plain. CNR, Progetto Finalizzato Geodinamica, Sottoprog. Modello Strutturale, Contrib. vol. 414. Milano: AGIP Publisher.

36. Piromallo, C., Morelli, A., 2003. P wave tomography of the mantle under the Alpine-Mediterranean area. Journal of Geophysical Research: Solid Earth 108.

37. Rawlinson, N., Urvoy, M., 2006. Simultaneous inversion of active and passive source datasets for 3-D seismic structure with application to Tasmania. Geophysical Research Letters 33.

38. Sambridge, M.S., Kennett, B.L., 2001. Seismic event location: nonlinear inversion using a neighbourhood algorithm. Pure Appl Geophys 158, 241-257.

39. Schaeffer, A., Lebedev, S., 2013. Global shear speed structure of the upper mantle and transition zone. Geophysical Journal International 194, 417-449.

40. Schneider, F.M., et al., 2013, Seismic imaging of subducting continental lower crust beneath the Pamir: Earth and Planetary Science Letters, v. 375, p. 101–112, doi:10.1016/j.epsl.2013.05.015

41. Searle, M., Hacker, B. R., Bilham, R., 2001. The Hindu Kush seismic zone as a paradigm for the creation of ultrahigh-pressure diamond-and coesite-bearing continental rocks. J. Geol. 109, 143-153.

42. Solarino, S., Malusà, M.G., Eva, E., Guillot, S., Paul, A., Schwartz, S., Zhao, L., Aubert, C., Dumont, T., Pondrelli, S., Salimbeni, S., Wang, Q., Xu, X., Zheng, T., Zhu, R., 2018. Mantle wedge exhumation beneath the Dora-Maira (U)HP dome unravelled by local earthquake tomography (Western Alps). Lithos 296-299, 623-636.

43. Stern, R.J., 2004. Subduction initiation: spontaneous and induced. Earth Planetary Science Letters 226, 275-292.

44. Sun, W.J., Kennett, B.L.N., 2016a. Uppermost mantle structure of the Australian continent from Pn traveltime tomography. J Geophys Res-Sol Ea 121, 2004-2019.

45. Sun, W.J., Kennett, B.L.N., 2016b. Uppermost mantle P wavespeed structure beneath eastern China and its surroundings. Tectonophysics 683, 12-26.

46. Ustaszewski, K., Schmid, S.M., Fügenschuh, B., Tischler, M., Kissling, E., Spakman, W., 2008. A map-view restoration of the Alpine-Carpathian-Dinaridic system for the Early Miocene, Orogenic Processes in the Alpine Collision Zone. Springer, pp. S273-S294.

47. von Raumer, J.F., Bussy, F., Schaltegger, U., Schulz, B., Stampfli., G.M., 2013. Pre-Mesozoic Alpine basements - Their place in the European Paleozoic framework. Geol. Soc. Am. Bull., 125, 89-108.

48. Winterer, E. L., & Bosellini, A. (1981). Subsidence and sedimentation on Jurassic passive continental margin, Southern Alps, Italy. AAPG Bulletin, 65(3), 394-421.

49. Zhang, R. Y., Liou, J. G., Ernst, W. G., 2009. The Dabie–Sulu continental collision zone: a comprehensive review. Gondwana Research 16(1), 1-26.

50. Zhao, L., Paul, A., Guillot, S., Solarino, S., Malusà, M.G., Zheng, T.Y., Aubert, C., Salimbeni, S., Dumont, T., Schwartz, S., Zhu, R.X., Wang, Q.C., 2015. First seismic evidence for continental subduction beneath the Western Alps. Geology 43, 815-818.

51. Zhao, L., Paul, A., Malusà, M.G., Xu, X., Zheng, T., Solarino, S., Guillot, S., Schwartz, S., Dumont, T., Salimbeni, S., Aubert, C., Pondrelli, S., Wang, Q., Zhu, R., 2016. Continuity of the Alpine slab unraveled by high-resolution P wave tomography. Journal of Geophysical Research: Solid Earth 121, 8720-8737.

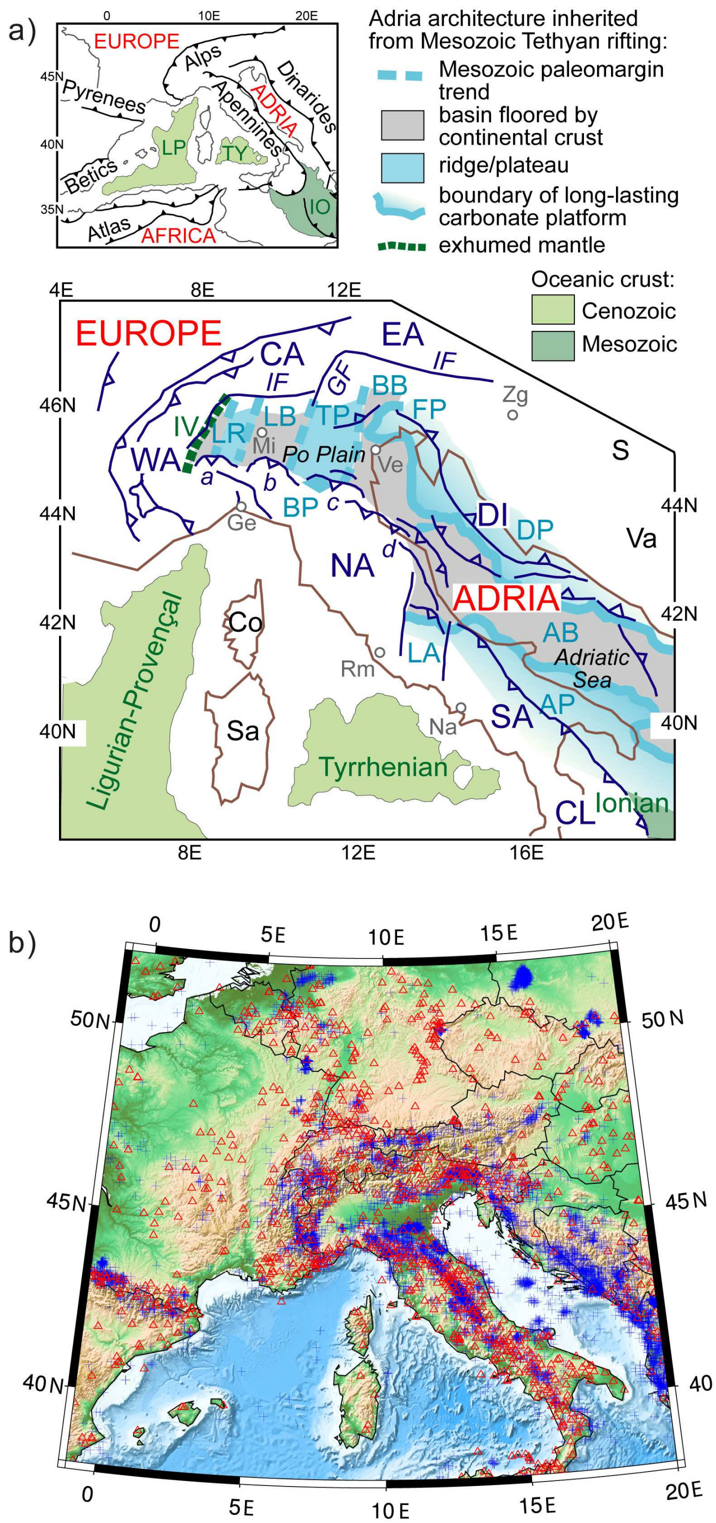

Figure 1. (a) Tectonic sketch map of the Central Mediterranean (top-left) and main tectonic structures of the Adriatic microplate. Tectonic domains: CA, Central Alps; DI, Dinarides; EA, Eastern Alps; IO, Ionian basin; LP, Ligurian-Provençal basin; NA,

Northern Apennines; SA, Southern Apennines; TY, Tyrrhenian basin; WA, Western Alps. Other keys: AB, Adriatic basin; AP, Apulian platform; BB, Belluno basin; BP, Bagnolo platform; Co, Corsica; DP, Dalmatia platform; FP, Friuli platform; GF, Giudicarie Fault; IF, Insubric Fault; IV, Ivrea body; LA, Latium-Abruzzi platform; LB, Lombardian basin; LR, Lugano ridge; S, Sava zone; Sa, Sardinia; TP, Trento plateau; Va, Vardar. Northern Apennine Thrust Fronts (a-to-d): a, Monferrato; b, Emilia; c, Ferrara-Romagna; d, Ancona. Main towns (in grey): Ge, Genoa; Mi, Milan; Na, Naples; Rm, Rome; Ve, Venice; Zg, Zagreb (based on Bigi et al., 1990; Jolivet et al., 2003; Kovács et al., 2007; Fantoni and Franciosi, 2010). **(b)** Location of seismic stations (red triangles) and seismic events (blue crosses) considered in this study (grey lines = country borders).

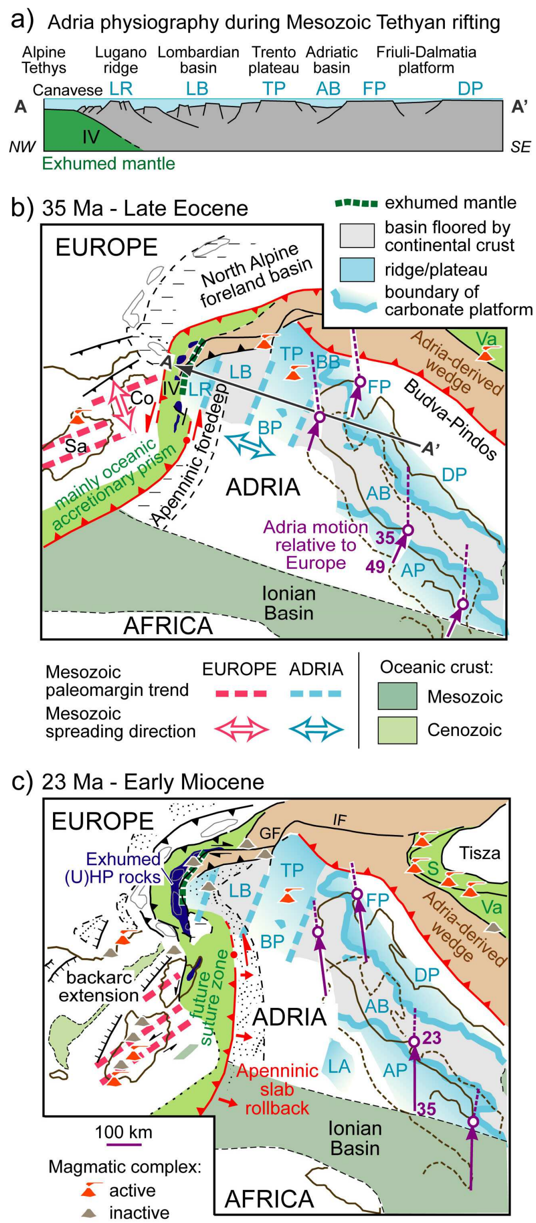

Figure 2. (a) Extensional architecture of the Adriatic microplate during Tethyan rifting, 2× vertical exaggeration, see location of cross-section in frame (b) (based on Winterer and Bosellini, 1981; Bertotti et al., 1993). **(b-c)** Palinspastic reconstruction of the Adria-Europe plate boundary zone during Eocene (U)HP rock exhumation in the Western Alps (b) and the onset of Apenninic slab rollback (c). Purple arrows indicate relative Adria-Europe relative plate motion (numbers = age in Ma). Acronyms as in Fig. 1. Based on Malusà et al. (2015) and Fig. 1, Ionian-Africa relationships after Faccenna et al. (2014).

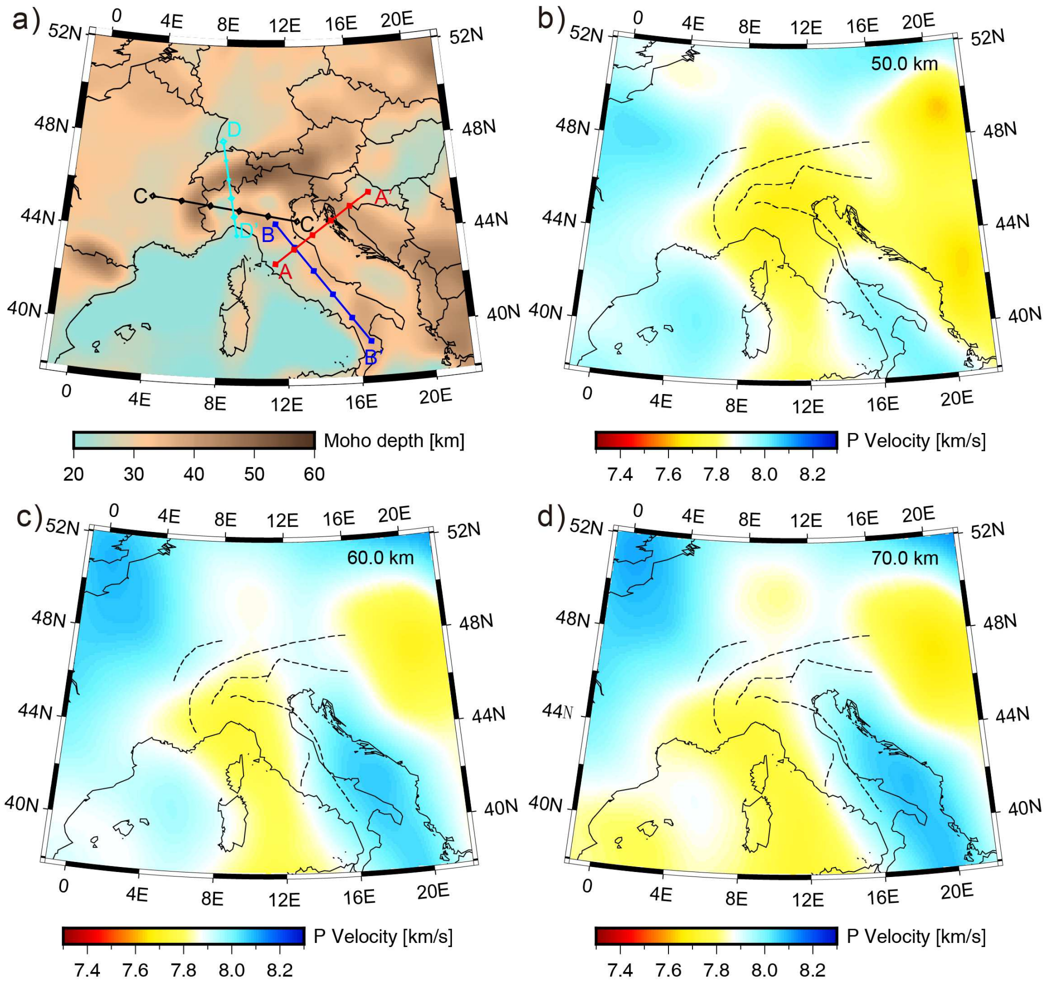

Figure 3. (a) Moho depth from Grad et al. (2009), and constructed P velocity model sliced at different depths: **(b)** 50 km, **(c)** 60 km and **(d)** 70 km. The initial model well reflects the broad scale of the geologic settings. Lines in color in Figure 3a show the locations of velocity cross-sections shown in Figure 8.

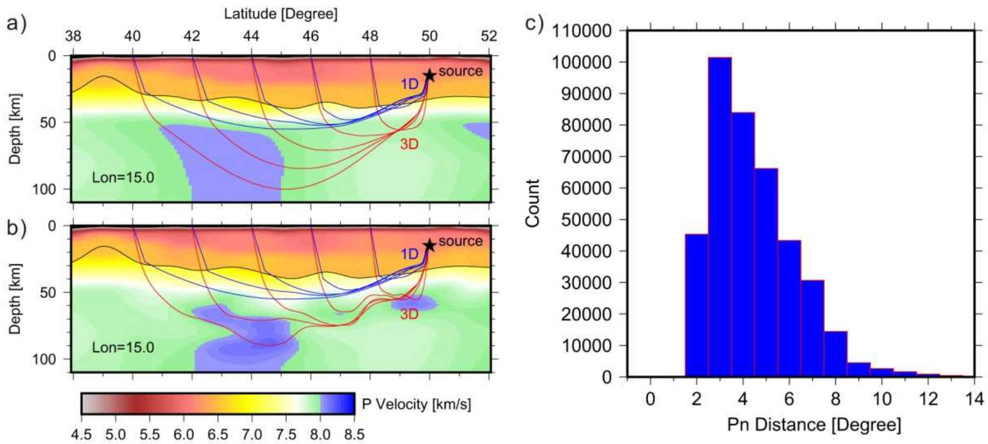

Figure 4. (a, b) Comparison of Pn raypaths between the 1-D ak135 model (blue lines) and the 3-D initial (a) and inverted (b) models (red lines), to which the sliced velocity profiles are referred to. **(c)** Histograms of Pn distances: most of them concentrates in ranges of 2—8°, which indicates that the zone shallower than 80 km is well sampled.

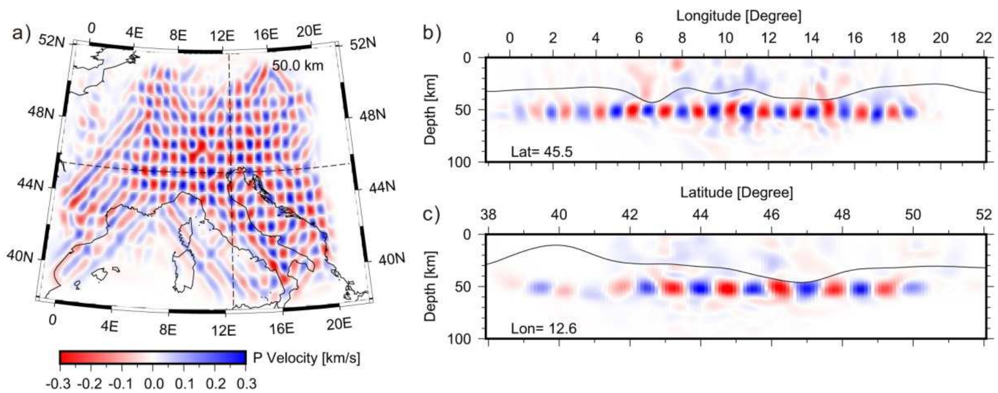

Figure 5. **(a)** Horizontal slice of the recovered checkerboard at depth of 50 km, and vertical slices along latitude of 45.5° **(b)** and longitude of 12.6° **(c)**. The resolution is 0.75°×0.75°. A layered velocity anomaly with 0.3 km/s is centred at depth of 50 km. The dashed lines in Figure 5a show the locations of vertical slices in Figure 5b and 5c.

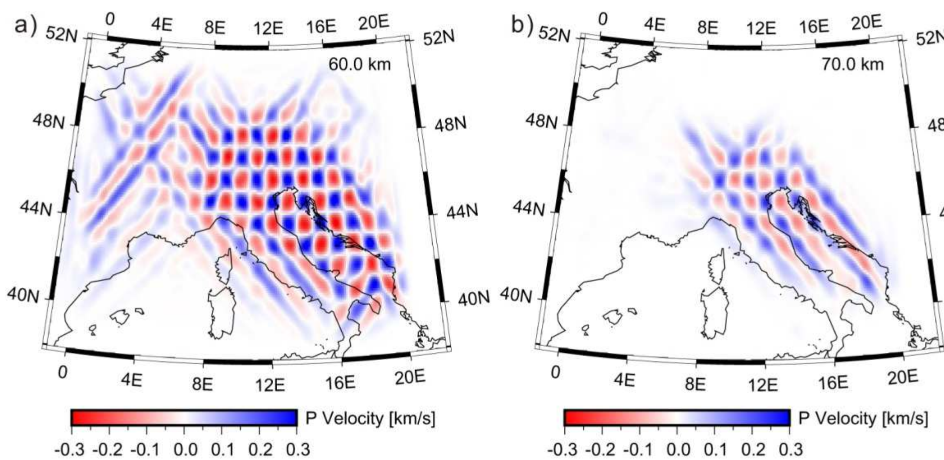

Figure 6. Recovered cherckerboard of resolution tests horizontal sliced at depth of **(a)** 60 km and **(b)** 70 km. A layered velocity anomaly with 0.3 km/s is centred at depth of 60 km in Figure 6a while the layer is centred at 70 km in Figure 6b. The resolution is 1°×1°.

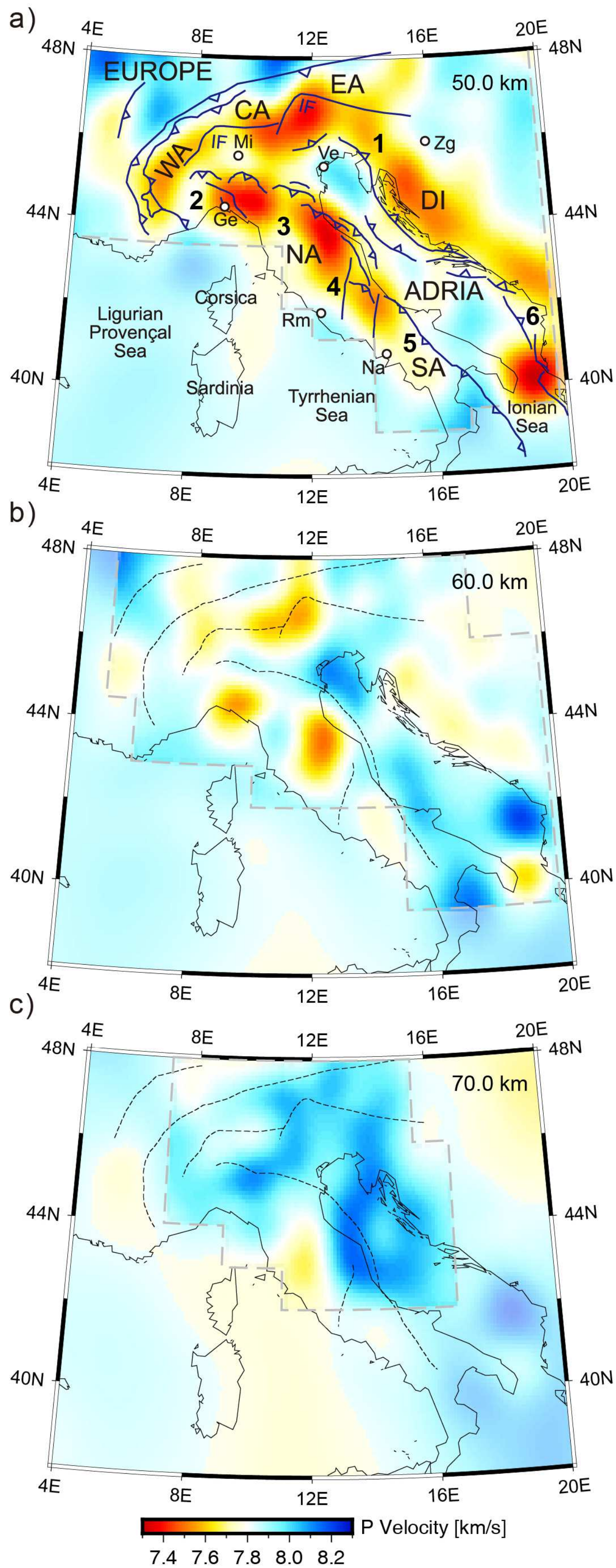

a)
b)
c)
50.0 km
60.0 km
70.0 km
4E
8E
12E
16E
20E
48N
44N
40N
EUROPE
EA
CA
WA
IF
Mi
Ve
Zg
DI
Ge
NA
ADRIA
1
2
3
4
5
6
Corsica
Ligurian Provençal Sea
Rm
Na
SA
Sardinia
Tyrrhenian Sea
Ionian Sea
P Velocity [km/s]
7.4 7.6 7.8 8.0 8.2

Figure 7. Horizontal slices of the inverted 3-D P wavespeed at different depths: **(a)** 50 km, **(b)** 60 km and **(c)** 70 km. Gray dashed lines delimit regions with good resolution (other regions are masked). Major tectonic lines and acronyms as in Figure 1a. Numbers 1 to 6 indicate the main features discussed in the text.

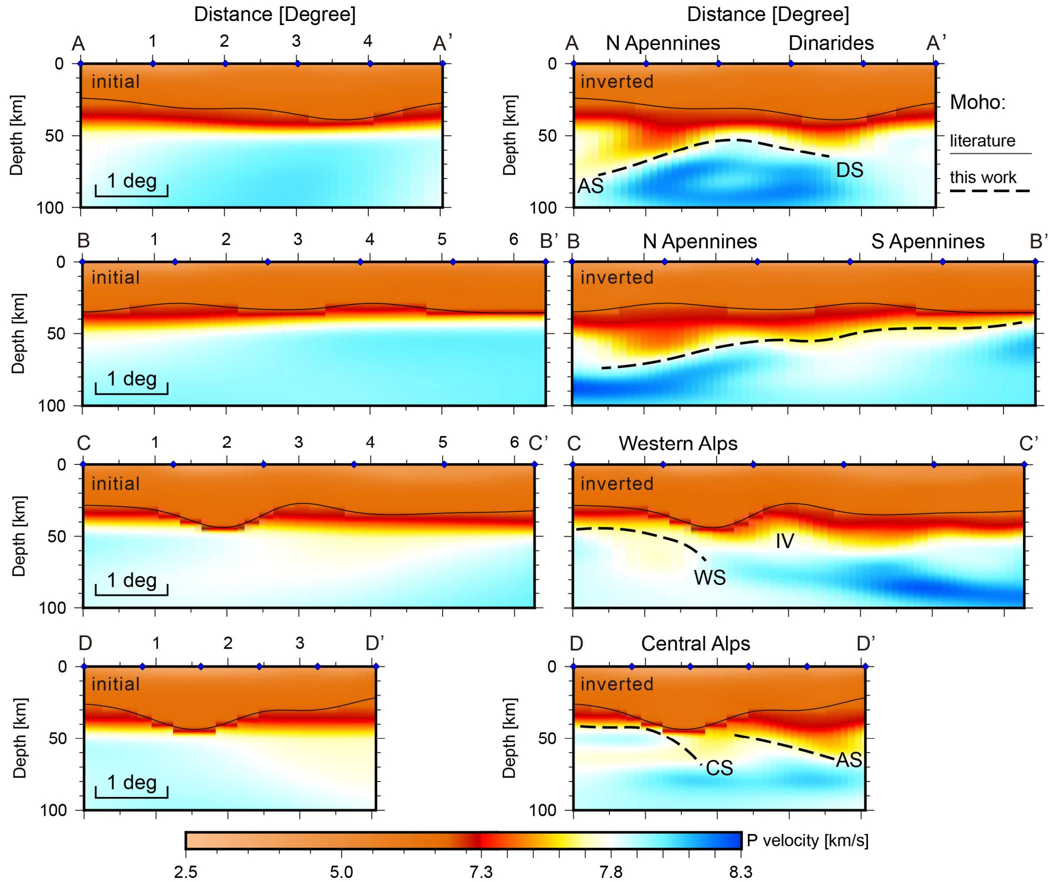

Figure 8. Vertical slices comparing the initial (left) and inverted (right) 3-D P wavespeed at different locations (~2× vertical exaggeration, see locations in Fig. 3a). The thin black line is the Moho as compiled from the literature. Note the opposite dipping subductions beneath the Apennines and the Dinarides (A-A'), the along-strike northward deepening of low P velocity along the Apennines (B-B'), the E-dipping subduction beneath the Western Alps (C-C'), and the S-dipping subduction beneath the Central Alps (D-D'). Acronyms: AS, Apenninic subduction; CS, Central Alps subduction; DS, Dinaric subduction; IV, Ivrea body; WS, Western Alps subduction.

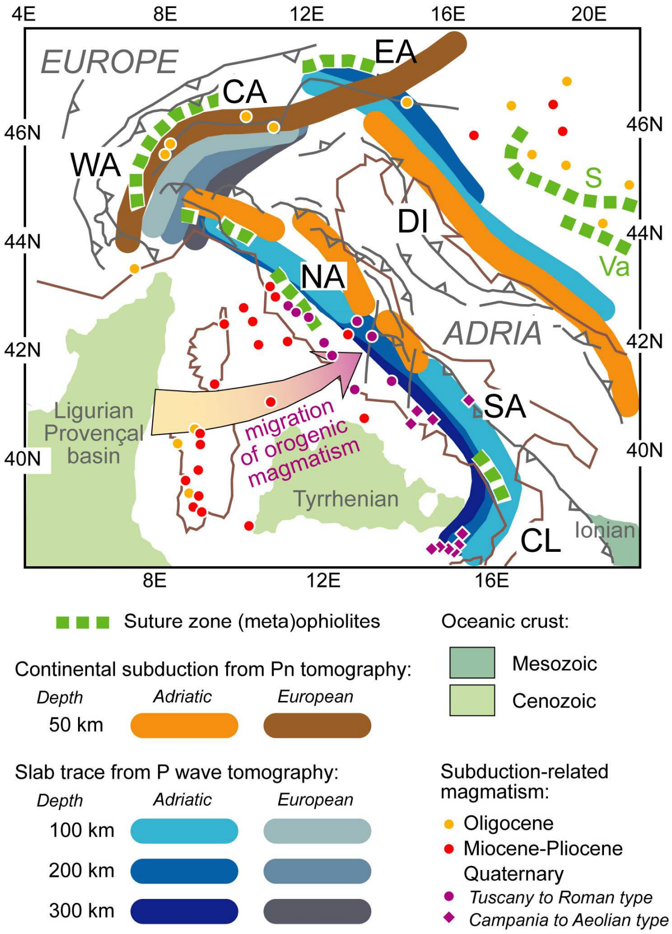

Figure 9. Relations between slab structure, distribution of orogenic magmatism (after Kovács et al., 2007; Carminati and Doglioni, 2012) and accreted (meta)ophiolites (after Bigi et al., 1990; Ustaszewski et al., 2008) around the Adriatic microplate. The present-day slab traces at 100, 200 and 300 km depth are based on P wave tomography models of Zhao et al. (2016) and Piromallo and Morelli (2003) (which was only considered outside of the well-resolved areas of the Zhao et al. (2016)'s model). Large arrow = migration of orogenic magmatism during Apenninic slab rollback. Acronyms: CA, Central Alps; CL, Calabria; DI, Dinarides; EA, Eastern Alps; NA, Northern Apennines; S, Sava zone; SA, Southern Apennines; Va, Vardar ophiolites; WA, Western Alps.

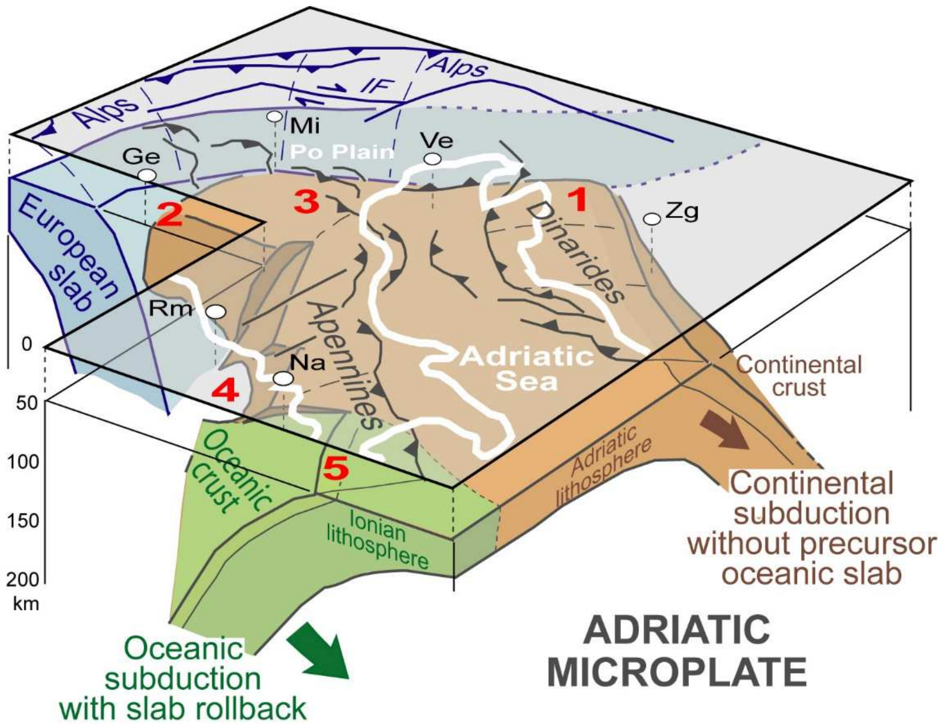

Figure 10. Cartoon summarizing the main features of the 3-D Pn tomography model of the Adriatic microplate. Continental subduction follows oceanic subduction in the Northern Apennines, whereas it takes place without a precursor oceanic slab beneath the Dinarides. In the lack of slab pull, the driving force to allow continental subduction beneath the Dinarides is likely provided by the northward motion of Africa. Acronyms as in Fig. 1a; numbers in red indicate the main features discussed in the text.